

RESEARCH ARTICLE

10.1002/2015JA021016

Key Points:

- First systematic study of hemispheric asymmetries of SAID
- SAID characteristics have clear north-south asymmetries
- SAID asymmetries are related to MIT, APP, and FAC

Correspondence to:

F. He,
hef@ciomp.ac.cn

Citation:

Zhang, X.-X., F. He, W. Wang, and B. Chen (2015), Hemispheric asymmetry of subauroral ion drifts: Statistical results, *J. Geophys. Res. Space Physics*, 120, 4544–4554, doi:10.1002/2015JA021016.

Received 15 JAN 2015

Accepted 7 MAY 2015

Accepted article online 11 MAY 2015

Published online 10 JUN 2015

Hemispheric asymmetry of subauroral ion drifts: Statistical results

Xiao-Xin Zhang¹, Fei He², Wenbin Wang³, and Bo Chen²
¹Key Laboratory of Space Weather, National Center for Space Weather, China Meteorological Administration, Beijing, China,

²Changchun Institute of Optics, Fine Mechanics and Physics, Chinese Academy of Sciences, Changchun, China, ³High-Altitude Observatory, National Center for Atmospheric Research, Boulder, Colorado, USA

Abstract A large database of more than 18,000 subauroral ion drift (SAID) events from DMSP observations from 1987 to 2012 is used to systematically investigate the features of SAID. SAID occurs mostly at $\sim 62^\circ$ – 60° magnetic latitude (MLAT) and $\sim 22:15$ – $22:45$ magnetic local time (MLT) for geomagnetically quiet conditions and at $\sim 58^\circ$ – 56° MLAT and $\sim 22:15$ – $22:45$ MLT for geomagnetically disturbed conditions in the North Hemisphere (NH)/South Hemisphere (SH), respectively. Significant north-south asymmetries in SAID occurrence, shape, and geomagnetic activity variations are found in this statistical study. The latitudinal width of a SAID is larger in the NH than in the SH. An interesting finding of this work is that the SAID occurrence probability peaks have an $\sim 180^\circ$ difference in longitude between the two hemispheres in the geographic coordinates for both geomagnetically quiet and disturbed conditions. The SAID width peaks in almost the same geomagnetic meridian zone with a geomagnetic longitude of $\sim 80^\circ$ – 120° in both hemispheres. Significant hemispheric asymmetries and spike signatures with sharp dips are found in all the latitudinal profiles of the horizontal velocities of SAIDs. The SAID is highly correlated to geomagnetic activity, indicating that the location and evolution of the SAID might be influenced by global geomagnetic activity, auroral dynamics, and the dynamics of ring currents.

1. Introduction

The rapid westward ion drifts (WIDs) and the corresponding large poleward electric fields (PEFs) in the nightside subauroral ionosphere were first named polarization jets (PJs) by Galperin *et al.* [1973] and subsequently called subauroral ion drifts (SAIDs) by Spiro *et al.* [1979]. Later, Foster and Burke [2002] suggested an inclusive name, subauroral polarization stream (SAPS), to encompass the SAID/PJ and the broader sunward plasma drifts in the subauroral region reported by Yeh *et al.* [1991].

Studies [Maynard *et al.*, 1980; Anderson *et al.*, 1991, 1993; Karlsson *et al.*, 1998; Figueiredo *et al.*, 2004; Huang and Foster, 2007; Puhl-Quinn *et al.*, 2007; He *et al.*, 2012, 2014] have found that SAIDs often appear as an intense plasma convection zone characterized by a latitudinally narrow ($\sim 1^\circ$ – 2°) and longitudinally elongated ($\sim 16:00$ – $03:00$ magnetic local time, MLT) region in the subauroral ionosphere with a WID peak speed of greater than 1000 m/s (corresponding to a PEF of ~ 30 mV/m). Voiculescu and Roth [2008] also reported abnormal SAID (ASAI) events, which have similar properties as above, except that the drifts are eastward. Statistical results by Liléo *et al.* [2010] have revealed that ASAI events occur mainly in the 23:00–03:00 MLT sector and between 65° and 70° in the corrected geomagnetic latitude at the equatorward of the auroral oval during geomagnetic quiet periods. WID was also observed in the dayside as reported by Freeman *et al.* [1992], but such dayside WID was defined as substorm-associated auroral surges which appear to be different from SAIDs. SAIDs are always located at the postdusk equatorial boundary of auroral electron precipitation and move to lower latitudes with increasing geomagnetic activity (K_p , Dst , and AE) [Karlsson *et al.*, 1998; Foster and Vo, 2002; He *et al.*, 2012] during substorms and especially during the substorm recovery phase [Anderson *et al.*, 1991; Karlsson *et al.*, 1998]. He *et al.* [2014] recently described solar cycle, seasonal, and diurnal variations of SAIDs using a large database of SAID events observed by the DMSP satellites.

The occurrence and characteristics of SAIDs [Anderson *et al.*, 1993, 2001; Karlsson *et al.*, 1998; He *et al.*, 2014] are closely related to auroral electron/ion precipitation, field-aligned currents (FACs), and ionospheric conductance, all of which have hemispheric asymmetries [Christiansen *et al.*, 2002; Hurlaud *et al.*, 2007; Luan *et al.*, 2010]. Anderson *et al.* [1991] analyzed two examples of SAID events observed by the ion drift meter on the Dynamic Explorer 2 satellite in conjugate hemispheres. They found that the geomagnetic latitudinal

positions of the WID peaks are different between the Northern Hemisphere (NH) and the Southern Hemisphere (SH). *Karlsson et al.* [1998] statistically investigated the north-south asymmetry of SAIDs using the electric field data from the Freja satellite. However, the database they used was small with less than 100 events. In a statistical study of the effect of SAPS on the thermosphere, *Wang et al.* [2011] used 2 years of ion velocity data from the DMSP ion drift meter (IDM) [Greenspan et al., 1986] and found significant asymmetries in the occurrence location and peak drift velocity of SAPS in the two hemispheres. However, the orbital sampling issue and the MLT distribution of the DMSP data were not considered in the statistical study of *Wang et al.* [2011]. Thus, it is difficult to obtain an overall understanding of the north-south asymmetry of SAPS. A case study using Super Dual Auroral Radar Network radars observations in both hemispheres by *Kunduri et al.* [2012] demonstrated that SAPS electric fields are different in the two hemispheres and these differences were attributed to the hemispheric asymmetry of ionospheric conductivity and the magnetic distortion effects.

Since SAIDs are commonly considered to be a subset of SAPS [Foster and Burke, 2002], it is expected that significant north-south asymmetry exists in the properties of SAIDs. For this purpose, the large SAID database developed by *He et al.* [2014] using DMSP observations from 1987 to 2012 has been used to systematically investigate the north-south asymmetries of SAIDs for the first time in this paper. We will examine the north-south asymmetry in the occurrence distribution, shape, drift velocity, and geomagnetic activity variations of SAIDs.

2. Database

A large database of 18,226 SAID events was compiled by *He et al.* [2014] from DMSP F8–F18 IDM [Greenspan et al., 1986] observations from 1987 to 2012. As we discussed in the Introduction section, the SAID is a strong westward ion drift that is confined in a latitudinally very narrow region just equatorward of auroral electron precipitation. The drift velocity of a SAID is typically larger than 1 km/s. In most of the studies of the SAID so far, the threshold for the peak drift velocity has been usually set to 1 km/s (corresponding to a poleward electric field of ~ 30 mV/m) [Anderson et al., 1991, 1993, 2001; Karlsson et al., 1998; Figueiredo et al., 2004; Mishin and Puhl-Quinn, 2007], although the original definition of a SAID in *Spiro et al.* [1979] was the sunward flow equatorward of the auroral zone with a speed that exceeds 500 m/s. Furthermore, it is commonly believed that the half width of SAID is less than 1.0° – 2.0° [Anderson et al., 1991, 1993, 2001; Freeman et al., 1992; Karlsson et al., 1998; Figueiredo et al., 2004; Mishin and Puhl-Quinn, 2007]. Thus, when compiling our SAID database, we used the following criteria [He et al., 2014]: (1) the horizontal WID peak exceeds 1000 m/s, (2) the latitudinal extent is less than 4.0° , (3) the event is located equatorward of the auroral zone in the dusk to midnight sectors, and (4) the poleward wall of the WID speed curve coincides with or is adjacent to the equatorial boundary of auroral precipitating electrons measured by the precipitating energetic particle spectrometer (Special Sensor Precipitating Electron and Ion Spectrometer (SSJ)/4 and SSJ/5) [Hardy et al., 1984]. This SAID database, along with geomagnetic indices of K_p , Dst , AE , and $ASY-H$, was used to statistically study the hemispheric asymmetries of SAID occurrence probability, configuration, and geomagnetic activity variations.

3. Statistical Results and Discussions

3.1. SAID Occurrence Probability

The distributions of the normalized SAID occurrence for $K_p < 4$ and $K_p \geq 4$ in both hemispheres are displayed in Figure 1 in a set of bins of MLT (0.5 h bins) between 16 and 02 h and MLAT (2.5° bins) between 50° and 70° in the NH and between -50° and -70° in the SH, respectively. There are 2175/7889 events for $K_p < 4$ and 2416/5746 events for $K_p \geq 4$ in NH/SH, respectively. It is noted that few SAID events are found after the midnight in the NH, in agreement with *Karlsson et al.* [1998].

Figure 1 shows that the maximum probabilities of the normalized SAID occurrence occur at $\sim 62^\circ$ MLAT and $\sim 22:15$ MLT for $K_p < 4$, and at $\sim 58^\circ$ MLAT and $\sim 22:15$ MLT for $K_p \geq 4$ in the NH, whereas in the SH the maximum probabilities of the SAID occurrence are at $\sim -60^\circ$ MLAT and $\sim 22:45$ MLT for $K_p < 4$ and at $\sim -56^\circ$ MLAT and $\sim 22:45$ MLT for $K_p \geq 4$. The maximum probability of the SAID occurrence can better describe the occurrence locations of SAIDs in the two hemispheres for different geomagnetic activity conditions [Figueiredo et al., 2004; He et al., 2014]. Figure 1 also shows that SAIDs in the SH occur generally at a location that is $\sim 2^\circ$ MLAT lower in MLAT and 0.5 h later in MLT than that in the NH. The normalized

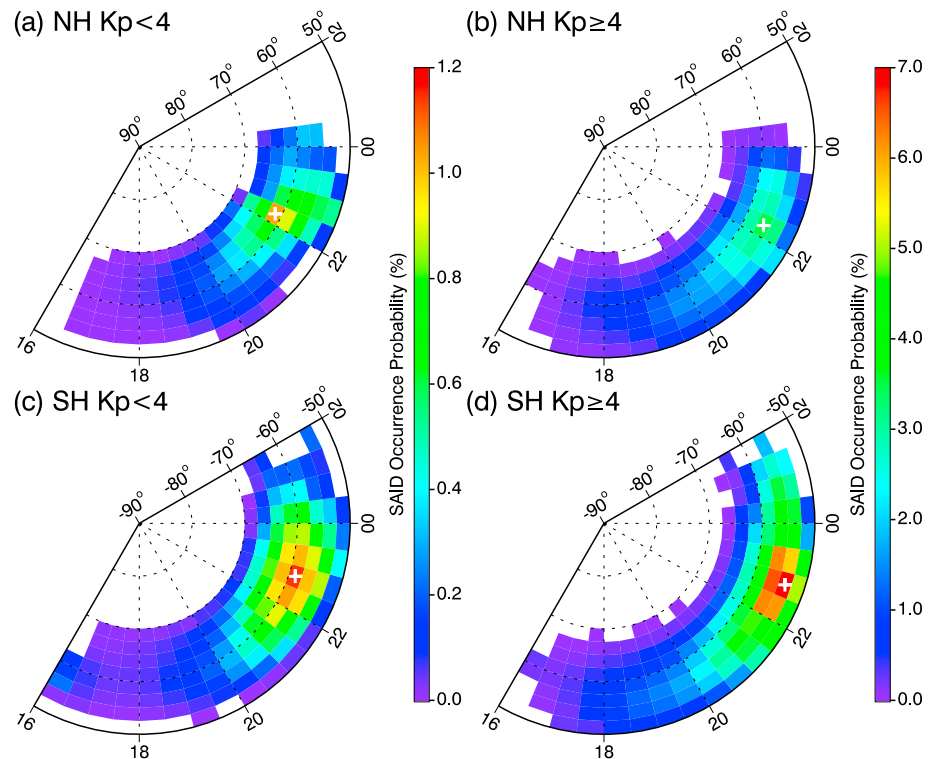


Figure 1. Contours of the (left column) numbers of orbital passes, (middle column) numbers of SAID events, and (right column) the normalized occurrence probabilities of SAID events in MLT and MLAT grids for geomagnetically quiet ($K_p < 4$) and disturbed ($K_p \geq 4$) conditions in NH/SH, respectively. The maximums in the right two columns are marked by the white crosses. Note that different scales are used for geomagnetically quiet ($K_p < 4$) and disturbed ($K_p \geq 4$) conditions.

occurrence probabilities for $K_p \geq 4$ are significantly larger than those for $K_p < 4$ in both hemispheres, demonstrating that the SAID occurs more often and more equatorward during geomagnetically disturbed periods compared with geomagnetically quiet periods. Figure 1 shows that SAIDs occur more frequently at premidnight of ~22:00–23:00 MLT. This is probably related to the fact that the midlatitude ionospheric trough (MIT) [He *et al.*, 2011; Lee *et al.*, 2011] is the deepest in this sector and that MIT is a precondition for the generation of SAIDs [Anderson *et al.*, 1993].

In order to further understand the regional/local distributions of the normalized SAID occurrences, we replot Figures 1b and 1d in a set of bins of geographic longitude (7.5° bins) between 180°W and 180°E and geographic latitude (2.0° bins) between 30° and 90° in the NH and between –30 and –90° in the SH for geomagnetically quiet ($K_p < 4$) and disturbed ($K_p \geq 4$) conditions in Figure 2. Figure 2 shows that the geographic latitudes of the SAID in the American sector in the NH and in the Oceania sector in the SH are significantly lower than those in the other sectors, which is probably due to the magnetic tilt effect. There are also obvious hemispheric asymmetries that normalized SAID occurrences in the geographic coordinates. The SAID occurs most frequently in the North Atlantic region in the NH and in the South Oceania region in the SH for both $K_p < 4$ and $K_p \geq 4$ conditions. There also appears a secondary occurrence peak near the South American sector for $K_p \geq 4$. There is an interesting phenomenon of the normalized SAID occurrence: in geomagnetic coordinates it peaks at premidnight of ~22:00–23:00 MLT in both hemispheres (Figures 1b and 1d), whereas in the geographic coordinates the maxima of the normalized SAID occurrence have an ~180° longitude difference between the two hemispheres. This phenomenon occurs for both geomagnetically quiet and disturbed conditions. Such a longitudinal difference in the normalized SAID occurrence needs further investigation in the future.

3.2. SAID Shape

The distributions of the latitudinal half width of SAIDs (SAID_{WH}) in MLT (binned in 0.5 h intervals between 16 and 02 h) and MLAT (binned in 2.5° intervals between 50° and 70° in the NH and between –50° and –70°

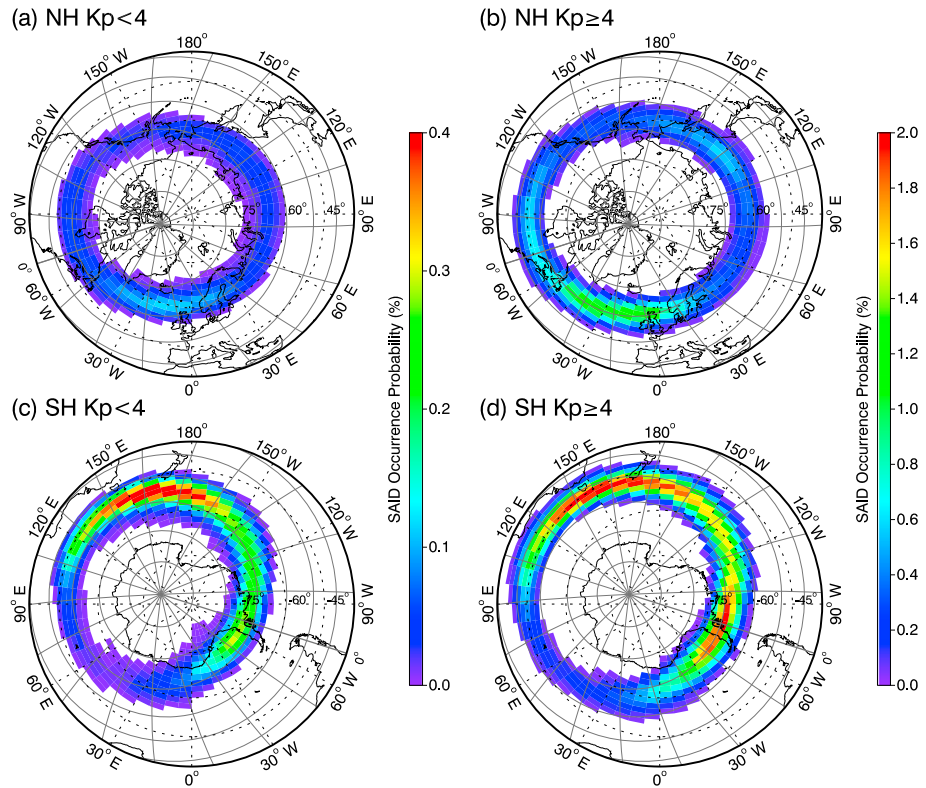


Figure 2. (a–d) Contours of the normalized SAID occurrence distribution in geographic longitude and latitude grids for geomagnetically quiet ($K_p < 4$) and disturbed ($K_p \geq 4$) conditions in NH/SH with different color scales, respectively. The gray grids in each panel represent the geomagnetic latitudes (10° intervals) and longitudes (20° intervals) with the thick gray lines to be 0° geomagnetic longitude. Note that different scales are used for geomagnetically quiet ($K_p < 4$) and disturbed ($K_p \geq 4$) conditions.

in the SH) for $K_p < 4$ and $K_p \geq 4$ are shown in Figure 3, respectively. The $SAID_W$ peaks at $\sim 19:00$ MLT and decreases from dusk to midnight in both hemispheres. It is also larger in the NH than in the SH. This is true for both $K_p < 4$ and $K_p \geq 4$ conditions. The average $SAID_W$ is 0.68° for $K_p < 4$ and 0.79° for $K_p \geq 4$ in the NH. The average $SAID_W$ is 0.51° for $K_p < 4$ and 0.69° for $K_p \geq 4$ in the SH. Figure 3 shows that $SAID_W$ increases with geomagnetic activity. During geomagnetically disturbed periods, both auroral particle precipitation and region-2 field-aligned currents (R2-FACs) become strong with wider latitudinal ranges, and more energy is transferred to the subauroral ionospheric region. Consequently, stronger frictional heating between the ions and the neutrals occurs [Anderson et al., 1993; Figueiredo et al., 2004]. Furthermore, the midlatitude electron density trough becomes deeper and wider. This can lead to a greater reduction of the height-integrated Pedersen conductivity in the subauroral region and cause a latitudinally wider WID region during geomagnetically active periods.

The MLT variations in Figure 3 clearly show the local time variations of $SAID_W$. Its regional characteristics are depicted in Figure 4. Figure 4 shows the distributions of $SAID_W$ in geographic longitudes (binned in 7.5° intervals between 180° W and 180° E) and latitudes (binned in 2.0° intervals between 30° and 90° in NH and between -30° and -90° in SH) for geomagnetically quiet ($K_p < 4$) and disturbed ($K_p \geq 4$) conditions, respectively. The $SAID_W$ is larger in the European region in the NH and in the South Indian Ocean region in the SH than in the other regions. It is also found that the $SAID_W$ peaks in almost the same geomagnetic meridian zone in both the NH and the SH in the geomagnetic longitude range of $\sim 80^\circ$ – 120° for both $K_p < 4$ and $K_p \geq 4$.

According to the selection criteria of SAIDs, the horizontal velocity of SAIDs is an important indicator of the strength of a SAID event. Figure 5 shows the averaged horizontal velocity profiles of SAIDs for $K_p < 4$ and $K_p \geq 4$ in different MLT sectors in both hemispheres, obtained by the following manner. The location of the

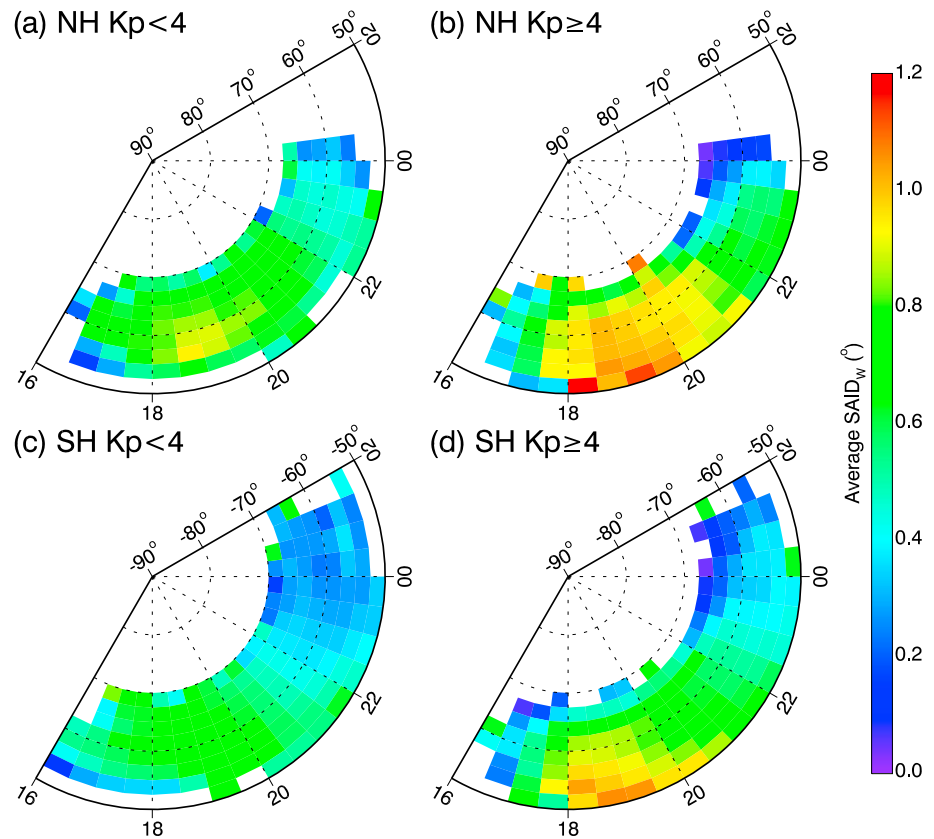


Figure 3. (a–d) Contours of the SAID_W for geomagnetically quiet ($Kp < 4$) and disturbed ($Kp \geq 4$) conditions in NH/SH, respectively.

WID peak is taken as the central MLAT of “0.” Each latitudinal velocity profile of a SAID centered at 0° is then resampled into the MLAT grids of 0.25° interval from 10° equatorward of the WID peaks to 10° poleward. A positive δ_{MLAT} (i.e., the MLAT of a horizontal velocity profile minus by the central MLAT) denotes poleward, and a negative one denotes equatorward. The velocities in each grid are finally averaged to obtain the SAID velocity profiles for all the events for different MLT sectors and geomagnetic activity levels.

The typical spike signatures of SAID [Anderson *et al.*, 2001] with sharp dips are found in all the horizontal velocity profiles in Figure 5 [Anderson *et al.*, 2001; Wang *et al.*, 2011]. These profiles also have significant hemispheric asymmetries. The westward horizontal drift velocities are larger in the NH than in the SH for $\delta_{\text{MLAT}} > 0^\circ$ in all MLT sectors for both $Kp < 4$ and $Kp \geq 4$ conditions. For $\delta_{\text{MLAT}} < 0^\circ$, however, the westward horizontal drift velocities are slightly larger in the NH than in the SH in all MLT sectors for $Kp < 4$ (Figures 5a–5d). However, they are almost the same in both hemispheres in all MLT sectors for $Kp \geq 4$ (Figures 5e–5h).

The drift velocity profiles for $\delta_{\text{MLAT}} < 0^\circ$ are smooth and change little in all the panels in Figure 5, whereas clear variations can be seen for $\delta_{\text{MLAT}} > 0^\circ$. For $Kp < 4$ and $\delta_{\text{MLAT}} > 0^\circ$, the velocity profiles in the NH gradually change from westward to eastward from dusk to midnight. Significant secondary dips in the profiles occur at $\delta_{\text{MLAT}} \approx 5^\circ$ in the 16:00–20:00 MLT sector (Figures 5a–5b). However, the velocity profiles in the SH are almost all eastward with no secondary dips (Figures 5a–5d). For $Kp \geq 4$ and $\delta_{\text{MLAT}} > 0^\circ$, the velocity profiles in both hemispheres gradually change from westward to eastward from dusk to midnight. And the secondary dips occur at $\delta_{\text{MLAT}} \approx 5^\circ$ in the 16:00–18:00 MLT sector (Figure 5e) in both hemispheres.

The WID peak velocities given in the bottom right corners in each panels in Figure 5 show that the peak velocity changes little with MLT but increases with geomagnetic activity. The peak velocities in the NH are generally slightly larger than those in the SH. The variations of the peak velocities with geomagnetic activity or hemisphere are not so evident as those of SAPS in Wang *et al.* [2011], possibly resulting from the fact that there are many events with WID peaks exceeding the IDM’s threshold of -3000 m/s, and the

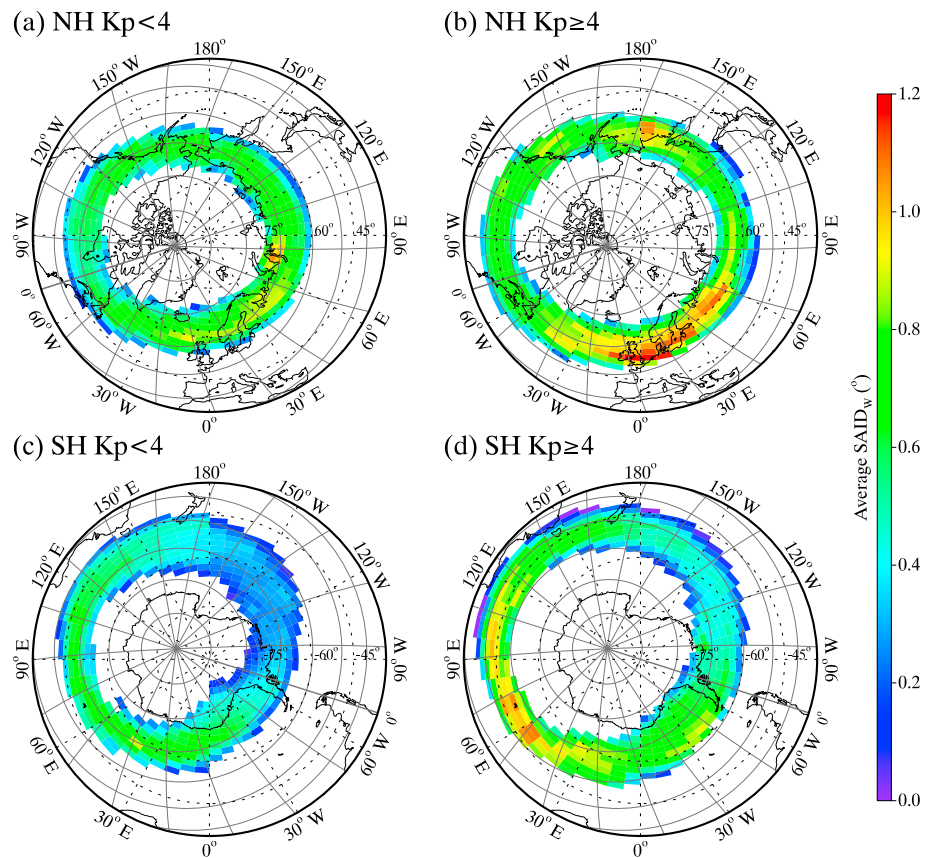


Figure 4. (a–d) Contours of the SAID_w in geographic longitude and latitude grids for geomagnetically quiet ($K_p < 4$) and disturbed ($K_p \geq 4$) conditions in NH/SH, respectively. The gray grids in each panel represent geomagnetic latitudes (10° intervals) and longitudes (20° intervals) with the thick gray lines to be 0° geomagnetic longitude and 60° geomagnetic latitude.

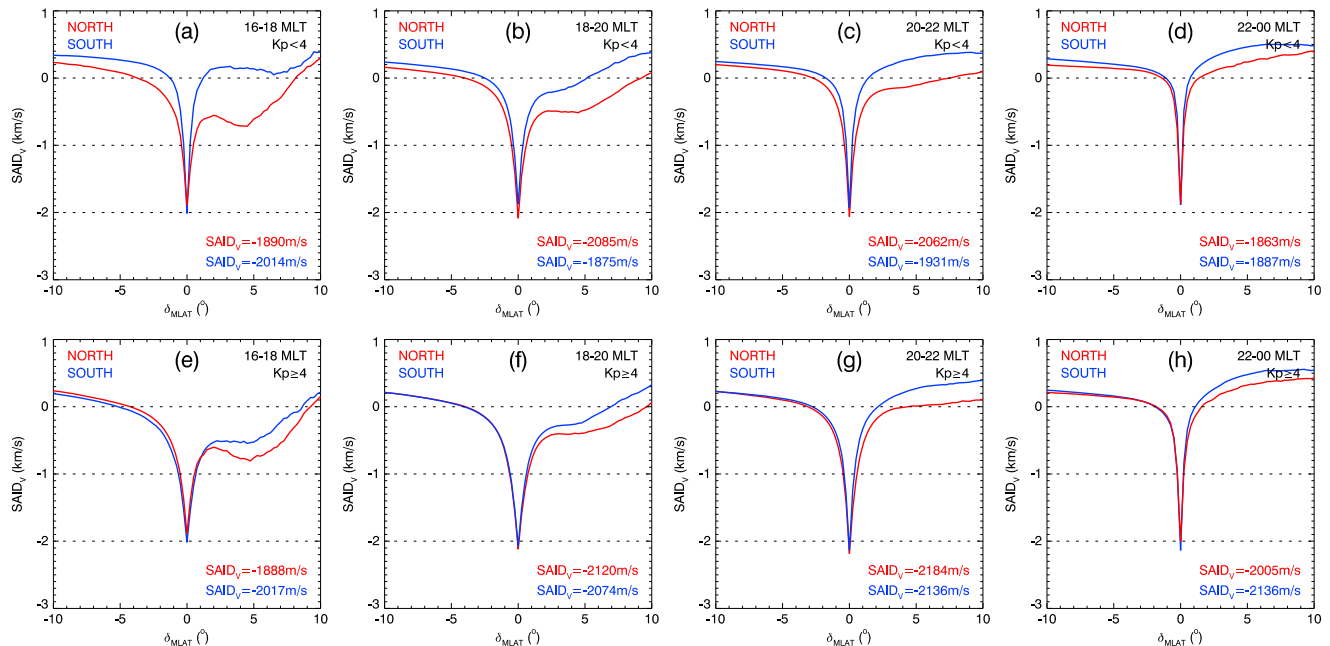


Figure 5. Averaged horizontal velocity profiles of SAID in both hemispheres in different MLT sectors, respectively. (a–d) Geomagnetically quiet conditions ($K_p < 4$) and (e–h) geomagnetically disturbed conditions ($K_p \geq 4$) are shown. Negative velocity denotes westward ion drifts.

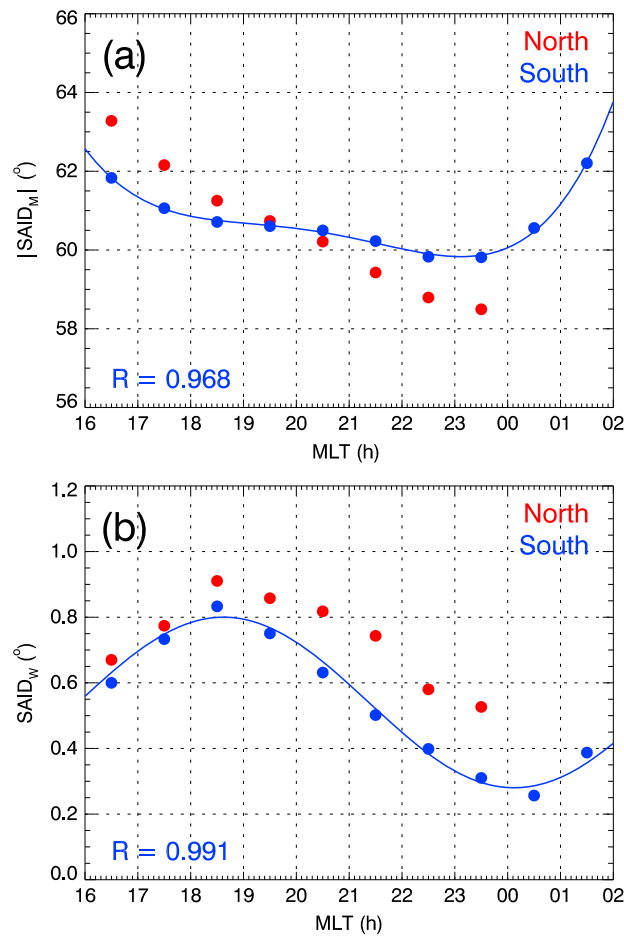


Figure 6. Dependences of (a) $|SAID_M|$ and (b) $SAID_W$ on MLT. The dots represent the averaged $|SAID_M|$ or $SAID_W$ in 1 h MLT intervals, and the curves represent the best fittings in SH, respectively. The coefficients of determination (R) for the fittings are shown at the bottom left corners of each panel.

intervals, and the curves represent the best fitted MLT variations. It is worth noting here that the postmidnight SAID events in the NH were not included in our analysis since the total number of events in the postmidnight sector is not large enough (only 10 events in the postmidnight sector compared with more than 120 events in other MLT sectors) to ensure a reasonable statistical significance level for the t test [Press *et al.*, 1992]. Since all postmidnight SAIDs in NH were rejected and no information can be given about the evolution of events after the geomagnetic midnight, the fittings are just done in SH for both $SAID_M$ and $SAID_W$ to avoid misleading under such circumstances. The fitted parameters for SH are listed in Table 1.

As illustrated in Figure 6a, the decrease of $|SAID_M|$ with MLT in the NH is faster than that in the SH at premidnight. This is related to the fact that the latitude of the MIT, which is the prerequisite for the generation of SAIDs [Anderson *et al.*, 1993], decreases faster with MLT in the NH [Lee *et al.*, 2011]. On the other hand, the increase of $|SAID_M|$ in the SH in the postmidnight sector might be caused by the increase

exact peak velocity is thus difficult to be determined [He *et al.*, 2014]. Furthermore, the SAID events in our database may be observed at different phases of their lifetimes which can be 0.5–3 h [Anderson *et al.*, 1991] and during which the peak velocity of the SAID may be highly dynamic and can change from -1000 m/s to -3000 m/s or more. It is thus possible that the peak velocity of a SAID event may be related to the different phases of its lifetime.

3.3. Geomagnetic Activity Variations

Statistical analysis thus shows clearly that geomagnetic activity has an important effect on the characteristics of SAIDs, especially the MLAT distributions of SAIDs ($SAID_M$) and $SAID_W$. Both parameters have significant variations. In this section, the hemispheric asymmetries of the geomagnetic activity dependence of $SAID_M$ and $SAID_W$ will be quantitatively investigated by normalizing them to a fixed MLT and then fitting their normalization to geomagnetic indices (Kp , Dst , AE , and $ASY-H$).

In order to normalize $SAID_M$ and $SAID_W$ to a fixed MLT, we need to obtain their distributions as functions of MLT first. Figure 6 shows the distributions of the averaged $SAID_M$ and $SAID_W$ in both hemispheres. The dots in Figure 6 are the averages of $|SAID_M|$ and $SAID_W$ in 1 h MLT

Table 1. Quality of Fits to $|SAID_M|$ and $SAID_W$ in SH

$ SAID_M ^a$					$SAID_W^b$			
a_0	a_1	a_2	a_3	a_4	b_0	b_1	b_2	b_3
1103.23	−206.496	15.309	−0.503	0.00618	0.26	0.57	3.5	0.54

^aFitting to quartic polynomial of $|SAID_M| = a_0 + a_1 \times MLT + a_2 \times MLT^2 + a_3 \times MLT^3 + a_4 \times MLT^4$.

^bFitting to sine function of $SAID_W = b_0 \times \sin(b_1 \times MLT + b_2) + b_3$.

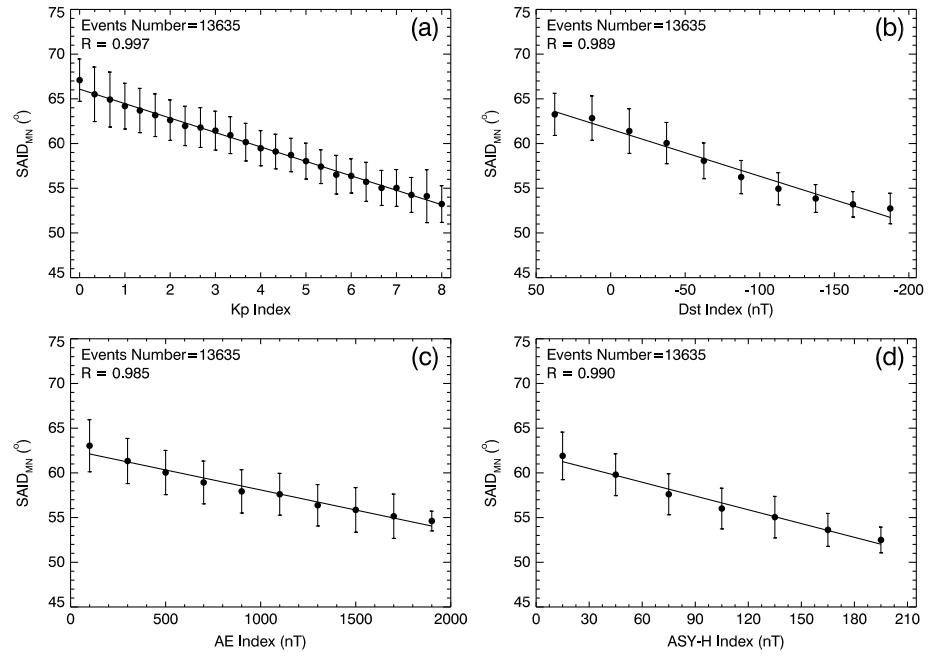


Figure 7. Fittings of the $SAID_{MN}$ to (a) Kp index, (b) Dst index, (c) AE index, and (d) $ASY-H$ index in SH. The closed circles represent the averaged $SAID_{MN}$ binned in $1/3$ for Kp , 50 nT for Dst , 200 nT for AE , and 30 nT for $ASY-H$, respectively, with standard deviations shown by the vertical bars. The total event number in SH and the coefficients of determination (R) are shown at the top left corners of each panel.

of the MLAT of the MIT there [Lee *et al.*, 2011]. Figure 6b shows that the variations of $SAID_W$ are typical sine functions of MLT in both hemispheres with peaks at ~ 19 h MLT and valleys at midnight.

Since all the SAID events in SH are observed in the 16:00–02:00 MLT sector, the center of the sector is at 21 h. This time is thus chosen to be the fixed MLT for normalizations of both $|SAID_M|$ and $SAID_W$. Based on the distribution functions fitted in Figure 6, $SAID_{MN} = |SAID_M| + a_1 \times (21 - T) + a_2 \times (21^2 - T^2) + a_3 \times (21^3 - T^3) + a_4 \times (21^4 - T^4)$

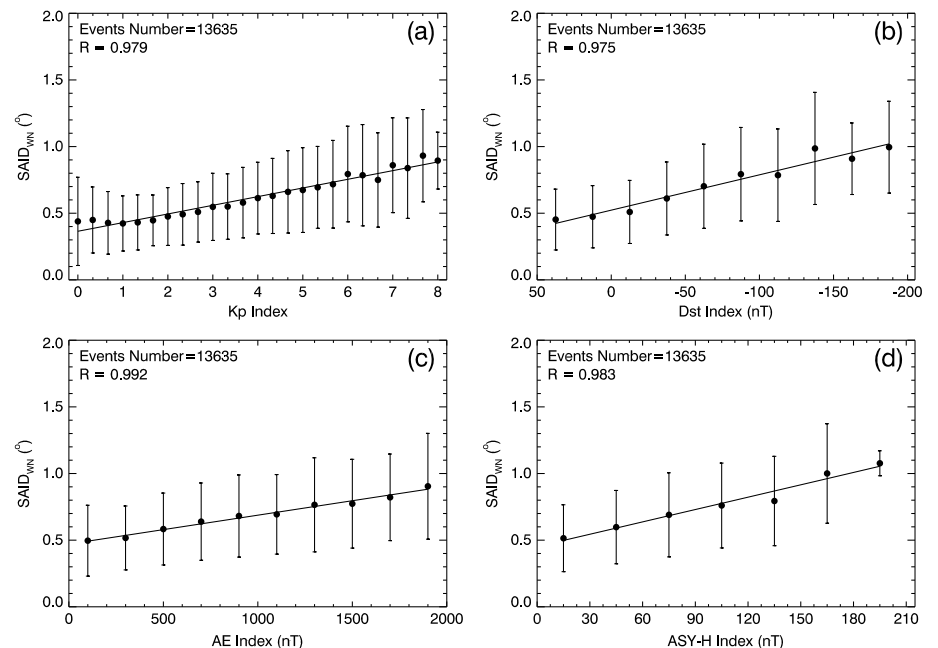


Figure 8. (a–d) Same as Figure 7 but for $SAID_{WN}$.

Table 2. Correlations of SAID_{MN} and SAID_{WN} to Various Geomagnetic Indices in SH

	SAID _{MN}			SAID _{WN}		
	A_0	A_1	R	A_0	A_1	R
Kp	66.08	−1.62	0.997	0.35	0.062	0.979
Dst	61.61	0.053	0.989	0.51	−0.0025	0.975
AE	62.57	−0.0045	0.985	0.46	0.00021	0.992
$ASY-H$	62.03	−0.051	0.990	0.45	0.0028	0.983

and $SAID_{WN} = SAID_W + 2 \times b_0 \times \cos[b_1 \times (21 + T)/2 + b_2] \times \sin[b_1 \times (21 - T)/2]$ are used to normalize $|SAID_M|$ and $SAID_W$ in SH, respectively. The coefficients a_1 , a_2 , a_3 , a_4 , b_0 , b_1 , and b_2 are listed in Table 1. Here $SAID_{MN}$ is the normalized $|SAID_M|$, $SAID_{WN}$ is the normalized $SAID_W$, and T is the MLT when a SAID event is measured, respectively.

$SAID_{MN}$ and $SAID_{WN}$ are fitted to geomagnetic indices (Kp , Dst , AE , and $ASY-H$) as shown in Figures 7 and 8, respectively. The dots in Figures 7 and 8 represent the averaged $SAID_{MN}$ and $SAID_{WN}$ binned in 1/3 intervals for Kp , 50 nT intervals for Dst , 200 nT intervals for AE , and 30 nT intervals for $ASY-H$, respectively. The standard deviations are given by the vertical bars. The colored lines represent the linear least squares fittings to the data in the form of $y = A_0 + A_1 \times x$, where y denotes $SAID_{MN}$ or $SAID_{WN}$ and x denotes Kp , Dst , AE , or $ASY-H$, respectively. The fitted values of A_0 , A_1 , and corresponding coefficients of determination (R) are listed in Table 2.

Figures 7 and 8 show that both $SAID_{MN}$ and $SAID_{WN}$ change linearly with Kp (Figures 7a and 8a), Dst (Figures 7b and 8b), AE (Figures 7c and 8c), and $ASY-H$ (Figures 7d and 8d) in SH. The large coefficients of determination listed in Table 2 ($R \approx 1$) indicate that SAIDs are highly correlated with geomagnetic activity and that the location and evolution of SAIDs might be influenced by global geomagnetic activity which is denoted by Kp , by the auroral dynamics which is described by the AE index, and by the R2-FACs which are related to the enhancement of symmetrical and partial ring currents which determine Dst and $ASY-H$ indices [Kunduri et al., 2012], respectively.

To understand the cause of the hemispheric asymmetries of SAIDs, we compare $SAID_V$ and $SAID_W$ with the estimated hemispheric power (HP) of auroral precipitation, cross-polar cap potential (CPCP), density of R2-FACs, and height-integrated Pedersen conductance (Σ_p) for the SAID database as shown in Table 3. For each SAID event, the corresponding estimated HP is obtained from the NOAA Space Environment Center, the CPCP is calculated using the Weimer's ionospheric electrodynamic model [Weimer, 2005] driven by the OMNI solar wind and interplanetary magnetic field parameters (http://omniweb.gsfc.nasa.gov/ow_min.html) that are time shifted from the bow shock to the polar region, the density of R2-FACs is calculated using the method described in He et al. [2014], and the height-integrated Σ_p is calculated using the flux and energy of the precipitating electrons observed by DMSP SSJ4/SSJ5 with the method of Robinson et al. [1987], respectively.

Table 3 shows that the estimated HP, the CPCP, and the density of R2-FACs in the NH are larger than those in the SH, whereas the height-integrated Σ_p is smaller in the NH. Note that a greater HP indicates stronger auroral precipitation energy flux and more energy input into the auroral region and a larger CPCP corresponds to stronger high-latitude convection electric fields which can accelerate particles more deeply into the inner magnetosphere and generate a larger density of R2-FACs. In addition, under the condition

Table 3. Average $SAID_V$, $SAID_W$, CPCP, Density of R2-FACs, Height-Integrated Σ_p and HP in NH and SH

Parameters	NH	SH
$SAID_V$ (m/s)	−2160	−2030
$SAID_W$ (deg)	0.67	0.50
HP (GW)	93	85
CPCP (kV)	92.3	86.5
Density of R2-FACs ($\mu A/m^2$)	0.14	0.08
Height-integrated Σ_p (mho)	6.96	8.21

that the MIT is deeper in the NH than in the SH [Lee et al., 2011], the ionospheric conductivity in the subauroral WID region is also lower in the NH, resulting a stronger R2-FAC and HP in the NH. Table 3 indicates that the field-aligned currents are stronger in the NH and they are closed through a lower-conductivity region [Anderson et al., 1993], and

the resultant frictional heating of subauroral ionospheric ions is stronger in the NH associated with deeper MIT and lower height-integrated Σ_p . Consequently, the WID region is wider in the NH than in the SH. The strength of WIDs is also stronger in the NH. This suggests that the hemispheric asymmetry of SAIDs is probably related to the hemispheric asymmetries in the magnetosphere and ionosphere. This is just a preliminary discussion for the hemispheric asymmetry of SAIDs, and the detailed relationships between SAID and MIT, HP, CPCP, R2-FAC, and Σ_p will be investigated in the future.

4. Conclusion

A large database of more than 18,000 SAID events from DMSP observations from 1987 to 2012 is used to systematically investigate the hemispheric asymmetries of SAIDs. Significant north-south asymmetries in SAID occurrence, shape, and geomagnetic activity dependence are found in this statistical study. The results are summarized as follows:

1. SAIDs occur mostly at $\sim 62^\circ$ – 60° MLAT and $\sim 22:15/22:45$ MLT for geomagnetically quiet conditions and at $\sim 58^\circ$ – 56° MLAT and $\sim 22:15/22:45$ MLT for geomagnetically disturbed conditions in NH/SH, respectively. An interesting finding is that the SAID occurrence peaks have $\sim 180^\circ$ longitudinal differences between the two hemispheres in the geographic coordinates for both geomagnetically quiet and disturbed conditions, indicating a strong regional/local dependence of the SAID occurrence.
2. The SAID_W peaks at $\sim 19:00$ MLT and decreases from dusk to midnight in both hemispheres. The SAID_W is larger in the NH than in the SH for both geomagnetically quiet and disturbed conditions. In addition, there is an interesting phenomenon that the SAID_W peaks in almost the same geomagnetic meridian zone of $\sim 80^\circ$ – 120° geomagnetic longitude in both hemispheres.
3. Significant hemispheric asymmetries are found in the latitudinal velocity profiles of SAIDs. The SAID velocity profiles also exhibit spike signatures with sharp dips. The westward drift velocities are generally larger in the NH than in the SH in all MLT sectors for geomagnetically quiet and disturbed conditions. The variations of the poleward wings of SAID velocity profiles are significantly different in the two hemispheres.
4. Fittings of both SAID_{MN} and SAID_{WN} to geomagnetic indices (K_p , Dst , AE , and $ASY-H$) indicate that SAID is highly correlated to geomagnetic activity. The location and evolution of SAIDs might be influenced by geomagnetic activity, auroral dynamics, and ring currents.

A preliminary investigation of the relationship between the strength of SAID and HP, CPCP, density of R2-FACs, and height-integrated Σ_p indicates that the hemispheric asymmetry of SAID is probably related to the hemispheric asymmetry of the magnetosphere and ionosphere. It is suggested that the hemispheric asymmetry in SAID is probably related to MIT [Lee *et al.*, 2011], auroral precipitation [Luan *et al.*, 2010], and field-aligned currents [Christiansen *et al.*, 2002, Kunduri *et al.*, 2012], all of which are north-south asymmetrical. The detailed relationships between SAID and MIT, HP, CPCP, R2-FAC, and Σ_p will be investigated in the future.

Acknowledgments

The authors would like to thank D.R. Weimer for providing the W05 electric field model. The authors sincerely thank the NOAA/NESDIS/National Geophysical Data Center for the provision of the DMSP IDM, SSJ/4, and SSM data and the NOAA/Space Environment Center for the provision of the hemispheric power data. The geomagnetic indices (K_p , AE , Dst , and $ASY-H$) are provided by the Kyoto World Data Center. This work was supported by the National Basic Research Program of China (2012CB957800 and 2011CB811400), the National Natural Science Foundation of China (41274147, 41204102, and 41229001), and the National Hi-Tech Research and Development Program of China (2012AA121000). The National Center for Atmospheric Research is sponsored by the National Science Foundation. Data are available upon request from the author at the following e-mail address: hef@ciomp.ac.cn.

Alan Rodger thanks Libo Liu and Mirela Voiculescu for their assistance in evaluating this paper.

References

- Anderson, P. C., R. A. Heelis, and W. B. Hanson (1991), The ionosphere signatures of rapid subauroral ion drifts, *J. Geophys. Res.*, **96**(A4), 5785–5792, doi:10.1029/90JA02651.
- Anderson, P. C., W. B. Hanson, R. A. Heelis, J. D. Craven, D. N. Baker, and L. A. Frank (1993), A proposed production model of rapid subauroral ion drifts and their relationship to substorm evolution, *J. Geophys. Res.*, **98**(A4), 6069–6078, doi:10.1029/92JA01975.
- Anderson, P. C., D. L. Carpenter, K. Tsunoda, T. Mukai, and F. J. Rich (2001), Multisatellite observations of rapid subauroral ion drifts (SAID), *J. Geophys. Res.*, **106**(A12), 29,585–29,599, doi:10.1029/2001JA000128.
- Christiansen, F., V. O. Papitashvili, and T. Neubert (2002), Seasonal variations of high-latitude field-aligned currents inferred from Ørsted and Magsat observations, *J. Geophys. Res.*, **107**(A2), 1029, doi:10.1029/2001JA900104.
- Figueiredo, S., T. Karlsson, and G. T. Marklund (2004), Investigation of subauroral ion drifts and related field-aligned currents and ionospheric Pedersen conductivity distribution, *Ann. Geophys.*, **22**, 923–934.
- Foster, J. C., and W. J. Burke (2002), SAPS: A new categorization for sub-auroral electric fields, *Eos Trans. AGU*, **83**(36), 393, doi:10.1029/2002EO000289.
- Foster, J. C., and H. B. Vo (2002), Average characteristics and activity dependence of the subauroral polarization stream, *J. Geophys. Res.*, **107**(A12), 1475, doi:10.1029/2002JA009409.
- Freeman, M. P., D. J. Southwood, M. Lester, T. K. Yeoman, and G. D. Reeves (1992), Substorm-associated radar auroral surges, *J. Geophys. Res.*, **97**(A8), 12,173–12,185, doi:10.1029/92JA00697.
- Galperin, Y. I., Y. N. Ponomarev, and A. G. Zosinova (1973), Direct measurements of ion drift velocity in the upper ionosphere during a magnetic storm, *Cosmicheskii Issled.*, **11**, 273–283.

- Greenspan, M. E., P. B. Anderson, and J. M. Pelagatti (1986), Characteristics of the thermal plasma monitor (SSIES) for the Defense Meteorological Satellite Program (DMSP) spacecraft S8 through S10, *Tech. Rep. AFGL-TR-86-0227*, Air Force Geophys. Lab., Hanscom Air Force Base, Mass.
- Hardy, D. A., H. C. Yeh, L. K. Schmitt, T. L. Schumaker, M. S. Gussenhoven, A. Huber, F. J. Marshall, and J. Pantazis (1984), Precipitating electron and ion detectors (SSJ/4) on the block 5D/Flights 6–10 DMSP satellites: Calibration and data presentation, *Tech. Rep. AFGL-TR-84-0317*, Air Force Geophys. Lab., Hanscom Air Force Base, Mass.
- He, M., L. Liu, W. Wan, and B. Zhao (2011), A study on the nighttime midlatitude ionospheric trough, *J. Geophys. Res.*, *116*, A05315, doi:10.1029/2010JA016252.
- He, F., X.-X. Zhang, B. Chen, and M.-C. Fok (2012), Plasmaspheric trough evolution under different conditions of subauroral ion drift, *Sci. China: Technol. Sci.*, *55*(5), 1–8, doi:10.1007/s11431-012-4781-1.
- He, F., X.-X. Zhang, and B. Chen (2014), Solar cycle, seasonal, and diurnal variations of subauroral ion drifts: Statistical results, *J. Geophys. Res. Space Physics*, *119*, 5076–5086, doi:10.1002/2014JA019807.
- Huang, C.-S., and J. C. Foster (2007), Correlation of the subauroral polarization streams (SAPS) with the Dst index during severe magnetic storms, *J. Geophys. Res.*, *112*, A11302, doi:10.1029/2007JA012584.
- Hurtaud, Y., C. Peymirat, and A. D. Richmond (2007), Modeling seasonal and diurnal effects on ionospheric conductances, region-2 currents, and plasma convection in the inner magnetosphere, *J. Geophys. Res.*, *112*, A09217, doi:10.1029/2007JA012257.
- Karlsson, T., G. T. Marklund, and L. G. Blomberg (1998), Subauroral electric fields observed by the Freja satellite: A statistical study, *J. Geophys. Res.*, *103*(A3), 4327–4314, doi:10.1029/97JA00333.
- Kunduri, B. S. R., J. B. H. Baker, J. M. Ruohoniemi, L. B. N. Clausen, A. Grocott, E. G. Thomas, M. P. Freeman, and E. R. Talaat (2012), An examination of inter-hemispheric conjugacy in a subauroral polarization stream, *J. Geophys. Res.*, *117*, A08225, doi:10.1029/2012JA017784.
- Lee, I. T., W. Wang, J. Y. Liu, C. Y. Chen, and C. H. Lin (2011), The ionospheric midlatitude trough observed by FORMOSAT-3/COSMIC during solar minimum, *J. Geophys. Res.*, *116*, A06311, doi:10.1029/2010JA015544.
- Liléo, S., T. Karlsson, and G. T. Marklund (2010), Statistical study on the occurrence of ASAD electric fields, *Ann. Geophys.*, *28*, 439–448.
- Luan, X., W. Wang, A. Burns, S. Solomon, Y. Zhang, and L. J. Paxton (2010), Seasonal and hemispheric variations of the total auroral precipitation energy flux from TIMED/GUVI, *J. Geophys. Res.*, *115*, A11304, doi:10.1029/2009JA015063.
- Maynard, N. C., T. L. Aggson, and J. P. Heppner (1980), Magnetospheric observation of large subauroral electric fields, *Geophys. Res. Lett.*, *7*(11), 881–884, doi:10.1029/GL007101p00881.
- Mishin, E. V., and P. A. Puhl-Quinn (2007), SAID: Plasmaspheric short circuit of substorm injections, *Geophys. Res. Lett.*, *34*, L24101, doi:10.1029/2007GL031925.
- Press, W. H., S. A. Teukolsky, W. T. Vetterling, and B. P. Flannery (1992), *Numerical Recipes*, Cambridge Univ. Press, Cambridge, U. K.
- Puhl-Quinn, P. A., H. Matsui, E. Mishin, C. Mouikis, L. Kistler, Y. Khotyaintsev, P. M. E. Décréau, and E. Lucek (2007), Cluster and DMSP observations of SAID electric fields, *J. Geophys. Res.*, *112*, A05219, doi:10.1029/2006JA012065.
- Robinson, R. M., R. R. Vondrak, K. Miller, T. Dabbs, and D. Hardy (1987), On calculating ionospheric conductances from the flux and energy of precipitating electrons, *J. Geophys. Res.*, *92*(A3), 2565–2569, doi:10.1029/JA092iA03p02565.
- Spiro, R. W., R. H. Heelis, and W. B. Hanson (1979), Rapid subauroral ion drifts observed by Atmospheric Explorer C, *Geophys. Res. Lett.*, *6*(8), 657–660, doi:10.1029/GL006i008p00657.
- Voiculescu, M., and M. Roth (2008), Eastward sub-auroral ion drifts or ASAD, *Ann. Geophys.*, *26*, 1955–1963.
- Wang, H., H. Lühr, K. Häusler, and P. Ritter (2011), Effect of subauroral polarization streams on the thermosphere: A statistical study, *J. Geophys. Res.*, *116*, A03312, doi:10.1029/2010JA016236.
- Weimer, D. R. (2005), Improved ionospheric electrodynamic models and application to calculating Joule heating rates, *J. Geophys. Res.*, *110*, A05306, doi:10.1029/2004JA010884.
- Yeh, H.-C., J. C. Foster, F. J. Rich, and W. Swider (1991), Storm time electric field penetration observed at mid-latitude, *J. Geophys. Res.*, *96*(A4), 5707–5721, doi:10.1029/90JA02751.